Exp. Theo. NANOTECHNOLOGY 4 (2020) 47– 58 https://doi.org/10.56053/4.3.47

TiO_2 nanorods with CdS quantum dots for optical applications

W. Jei[1], *J. Lim*[2,*], *H. Hoa*[3]

[1]School of Physics, State Key Laboratory of Crystal Materials, Shandong University, Jinan 250100, PR China

[2]School of Information Science and Engineering, Shandong University, Jinan 250100, PR China

[3]Department of Physics, Portland State University, Post Office Box 751, Portland, OR 97207-0751, United States

*) E-mail address: limj@sdu.edu.cn

Received 15/12/2019, *Accepted* 28/6/2020, *Published* 15/9/2020

We combine CdS semiconductor quantum dots and single-crystalline rutile TiO2 nanorod arrays to produce a practical quantum dot sensitized solar cell. A facile wet-chemical approach was implemented for growth of this CdS@TiO2 architecture. Rutile TiO2 nanorod arrays with lengths of 1–2 mm and diameters of 40–60 nm was synthesized on fluorine-doped tin oxide glass by a hydrothermal process in a titanium tetrachloride precursor solution. CdS quantum dots with a size of 5–10 nm was deposited onto a TiO2 nanorod surface using an ultrasonic-assisted chemical bath deposition method. The resulting CdS quantum dots and TiO2 nanorods formed a type-II heterojunction and showed increased absorption over visible light range. Incident photon-to-current conversion efficiencies (IPCE) as high as 85% and power conversion efficiencies of 2.54% were obtained using a polysulfide electrolyte.

Keywords: II-VI; QDs; Optical.

1. INTRODUCTION

Novel approaches to utilize solar energy have attracted great attention world-wide. Being a fast-growing source of clean energy solution, Si-based solar cells could provide ample power at a moderate price; the search for an efficient alternative photovoltaic (PV) system still remains a serious challenge. In order to achieve better efficient use of solar energy, many new PV systems have been introduced, including dye-sensitized solar cells (DSSC), organic solar cells, and multi-junction solar cells. Most of these strategies employ the following working principles: (i) absorption of a high energy photon and subsequent generation of an electron–hole pair. (ii) Charge separation occurs, so the electrons and holes are separated across a heterojunction and (iii) charges are transported to load. To achieve higher photocurrent efficiency, the loss during each step must be minimized. One classical example is the architecture of a DSSC [1,2]. Light is absorbed by dye pigments on the interface between the semiconducting material and conducting liquid electrolyte, the dye molecules become excited and generate hot electrons, which are subsequently transported by the semiconducting material

to the electrode. Another example is the conjugated polymer photovoltaic cells in which two or more photovoltaic materials are blended to form a three-dimensional continuous network structure. In this case the light is absorbed by all materials, and photo- generated electron–hole pairs are quickly separated and transported across the nearby interfacial boundaries. Both organic solar cells [3–6] and multi-junction solar cells [7–9] have been constructed to demonstrate this approach. Despite the success of the above-mentioned solar cells, new material application and architecture configuration still need to be discovered to improve performance and reduce the cost of solar cells.

To improve charge transport, single-crystalline wide band gap materials, such as TiO_2, can be used as a direct pathway from the light absorbing material to the conducting electrode, thereby increasing the photocurrent efficiency [10]. Single crystalline TiO_2 nanorods grown directly on transparent conductive oxide (TCO) electrodes provide a perfect solution by avoiding particle-to-particle hopping that occurs in poly- crystalline films. In addition, the band gap of TiO_2 provides a suitable substrate for visible light transmission and is an ideal material to form a type-II heterojunction with narrow band gap sensitizing materials such as CdS and CdSe. Moreover, the high stability of TiO_2 in corrosive electrolytes makes it a superior choice when weighed against other wide-gap semiconductors such as ZnO [11].

The solar spectrum, containing photons ranging from 0.5 to 3.5 eV, limits the intrinsic practicality of such wide- gap semiconductors because low-energy photons are not absorbed. In conventional tandem solar cell that consists of wide-gap and narrow-gap semiconducting materials, considerable number of high-energy photons dissipate excess energy in the form of heat in the narrow-gap semiconducting material. The use of quantum dots (QD) such as CdS, CdSe, InP, and PbSe to produce more than one electron–hole pair per single absorbed photon, also known as multiple exciton generation (MEG) [12–15], is a promising solution to enhance absorbance efficiency. In addition to the utilization of the MEG phenomenon, CdS QDs offer the ability to adjust absorption spectra by tuning QD sizes to match the solar spectrum [16,17]. Furthermore; the crea- tion of a type-II heterojunction by growing CdS QDs on the TiO_2 surface greatly enhances charge separation.

To date, CdS@TiO_2 nanostructured solar cells have been reported by several groups. While most of the reported works were conducted on polycrystalline TiO_2, [18,19] few works were conducted on TiO_2 single crystalline nanorods [20]. In addition, most growth methods relied on vapor phase techniques [21,22] that require high operating temperatures. Compared to vapor phase techniques, wet-chemical appro- aches are more suitable for inexpensive mass production and offer better control over morphology. Recently, there has been several reports on attaching QDs onto various

TiO_2 surfaces using different methods: (i) synthesized QDs attached to TiO_2 surfaces with linker molecules [23,24]; (ii) QDs grown directly onto TiO_2 surfaces using successive ionic layer absorption (SILAR) method [16,25]; (iii) QDs grown directly onto TiO_2 surfaces by chemical bath deposition (CBD) approach [26,27]. With the first method, size of QDs can be more readily controlled and QD obtained are of higher quality compared to other methods; however, due to the low coverage on the electrode surface, low power conversion efficiency is achieved. The latter approaches obtained high coverage of the electrode surface with a

nucleation and growth mechanism, but rendering it difficult to control the size distribution of QDs and subsequently unable to adjust absorption of spectra to enhance visible light absorption. We used an ultrasound assisted CBD method, which extensively increased CdS QDs growth speed compared to traditional CBD approach also size distribution is more optimized. In our work, there is negligible redshift with increase of CBD cycles suggesting that size growth of CdS QDs is being impeded while achieving a higher surface coverage.

In this article, we introduce an entirely wet-chemical approach toward building a quantum dot sensitized solar cell (QDSSC) with CdS@TiO_2 architecture. QDSSC structures are fabricated using CdS QD sensitizers and TiO_2 nanorods grown directly on fluorine-doped tin oxide (FTO) substrates. A low temperature (1801C) wet-chemical technique was used to grow ordered TiO_2 nanorod arrays directly on FTO glass followed by a facile ultrasound-assisted chemical bath deposition (CBD) of CdS QDs onto rutile single crystalline TiO_2 nanorods. Using this QDSSC, an IPCE as high as 85% can be obtained in the visible light region with a power conversion efficiency of 2.54%.

2. EXPERIMENTAL

TiO_2 nanorod arrays were grown directly on fluorine-doped tin oxide (FTO) coated glass substrates by the following hydro- thermal method: 35–50 mL of deionized water was mixed with 55–40 mL of concentrated hydrochloric acid (HCl, 36–38% by weight, Sinopharm) to reach a total volume of 90 mL in a stainless-steel autoclave with a Teflon container cartridge. The mixture was stirred at ambient conditions for 5 min, and then 300–1000 mL of titanium tetrachloride ($TiCl_4$, 99.9%, Aladdin) was added. After stirring for another 5 min, FTO substrates (2 3 cm, 8–12 O/sq), ultrasonically cleaned for 10 min in a mixed solution of deionized water, acetone, and 2-propanol with volume ratios of 1:1:1, were placed at an angle against the Teflon container wall with the conducting side facing down. The hydrothermal synthesis was conducted at 180 1C for 2 h in an electric furnace. After synthesis, the autoclave was cooled to room temperature under flowing water, which took approximately 5 min. The FTO substrate was taken out, washed extensively with deionized water and allowed to air dry.

CdS QDs were deposited onto the TiO_2 nanorod surface by chemical bath deposition (CBD). Before the CBD process, solutions of 0.5 M cadmium nitrate ($Cd(NO_3)_2$) and 0.5 M sodium sulfide (Na_2S) were prepared by dissolving $Cd(NO_3)_2$ in ethanol and Na_2S in methanol. A typical CBD cycle involved dipping the FTO, glass pre-grown with TiO_2 nanorods, in Na_2S solution for 10 min, rinsing in methanol, then dipping it for another 10 min in $Cd(NO_3)_2$, and rinsing again in ethanol. The entire CBD process was carried out under ultrasonic agitation (40 kHz, 60 W) with the TiO_2- coated substrate facing downward and placed at an angle against the beaker wall.

The samples were characterized by X-ray diffraction (XD-3, PG Instruments Ltd.) with Cu Ka radiation (l=0.154 nm) at a scan rate of 21 min^{-1}. X-ray tube voltage and current were set at 36 kV and 20 mA, respectively. The morphological and lattice structural information was determined by field emission scanning electron microscopy (FESEM, Hitachi S-4800) and transmission electron microscopy (TEM, JEOL JEM-2100).

Exp. Theo. NANOTECHNOLOGY 4 (2020) 47-58

CdS quantum-dot sensitized solar cells (QDSSC) were assembled using CdS@TiO_2 structure. Pt counter electrodes were prepared by coating a thin layer of Pt on FTO glass using magnetron sputtering. Then, a 60 mm thick sealing material (SX-1170-60, Solaronix SA) with a 3 3 mm aperture was pasted onto the Pt counter electrodes. The CdS@TiO_2 sample and Pt counter electrode were sandwiched and sealed with the conductive sides facing inward. A redox electrolyte was injected into the space between the two electrodes. In this study, a polysulfide electrolyte was used. The liquid electrolyte was composed of 0.5 M Na_2S, 2 M sulfur and 0.2 M KCl (all from Sinopharm) mixed solution of deionized water and ethanol with volume ratios of 35:65.

A solar simulator (Model 11000Abet Technologies) with an AM1.5 filter was used to illuminate the working solar cell at light intensity of 1 sun (100 mW/cm^2). A sourcemeter (2400, Keithley) was used for electrical characterization during the measurements. The incident photon-to-current conversion efficiency (IPCE) measurements were carried out with a custom measurement system consisting of a 150 W Xe lamp (LSH-X150, Zolix), monochromator (7ISW30, 7-Star) and a sourcemeter (2400, Keithley). The measurements were carried out without bias illumination with respect to a calibrated OSI standard silicon solar photodiode. UV–visible transmission spectra of the prepared samples were analyzed using a UV–visible spectrometer (TU-1900, PG Instruments, Ltd.).

3. RESULTS AND DISCUSSION

3.1 Growth of single-crystalline rutile TiO_2 nanorods

It is known that wet-chemical techniques are preferred as an ideal process for growing nanostructured materials because the particle size, morphology, and structure can be easily controlled by adjusting preparation parameters. Also, single-crystalline materials are easily obtained through hydrothermal approach. Ordered TiO_2 nanostructures with different morphologies, such as nanoparticles [28], nano- wires [29], and nanotubes [30], have been synthesized by different hard-template methods. Alternative wet-chemical techniques for crystalline TiO_2 growth and morphology control are also an interesting and promising subject.

In our study, we found that the morphology of the TiO_2 nanorods could be adjusted to preferred conditions by varying solution acidity and precursor concentration. The decrease in nanorod diameter and density is evident with an increase in solution acidity and decrease in precursor

concentration (Fig. 1). At a low concentration of titanium tetrachloride ($TiCl_4$) precursor, slim rod (0.3 mL) and thick rod (0.4 mL) crystals are obtained (Fig. 1a and b). When the concentration of $TiCl_4$ is increased to 0.5 M, the formation of long thick rods with diameters of 100–300 nm and lengths up to 5 mm (Fig. 1c and d) is observed. When the quantity of precursor was increased to 1.0 mL, a continuous network of TiO_2, consisting of densely packed TiO_2 nanorods, was observed (Fig. 1e). When the volume ratio of hydrochloric acid and deionized water was decreased from 40:50 (Fig. 1a) to 35:55 (Fig. 1f), the TiO_2 nanorod diameter increased dramatically.

Exp. Theo. NANOTECHNOLOGY 4 (2020) 47-58

To fully utilize the advantage of the TiO_2 nanorod arrays for better light absorbance, a suitable nanorod spacing and diameter must be determined; the density of TiO_2 nanorods should be maximized while preserving enough space for CdS quantum dot deposition. Smaller nanorod diameters are desirable for increasing the sensitized surface area per unit substrate area, which enhances light absorption. The optimal performance was found with a TiO_2 nanorod growth solution composed of 340 mL $TiCl_4$, 40 mL hydrochloric acid, and 50 mL deionized water, reaching a total volume of 90 mL.

TiO_2 nanorods were successfully grown on FTO-coated glass substrates at 180 1C for 2 h. Field emission scanning electron microscopy (FESEM) images of top and cross-sectional views are shown (Fig. 2a and b). The images at different locations and viewing angle reveal that the entire surface of the FTO- coated glass substrate is uniformly covered with ordered TiO_2 nanorods. Fig. 2d shows a high magnification FESEM image of the nanorods, which are typically 40–60 nm in diameter and 1–2 mm in length. The density of nanorods is typically 20 nanorods/mm^2 with an average spacing of 200 nm. The nanorods are tetragonal in shape with square top facets consisting of many small grids. X-ray diffraction (XRD) patterns show that the TiO_2 grown on the FTO-coated glass substrates have a tetragonal rutile structure [SI 1]. Compared to powdered rutile TiO_2 XRD patterns, the (002) diffraction peak was significantly enhanced, and some diffraction peaks including (101), (110), and (211) were absent, which indicates that the TiO_2 nanorods are highly oriented with respect to the substrate surface normal and that the TiO_2 nanorods grow in the (001) direction with the growth axis perpendicular to the substrate surface. A TEM image and a corresponding selected area electron diffraction (SAED) pattern indicate high crystallinity of the TiO_2 nanorods (Fig. 2c). The reason that the hydrothermal growth method delivers rutile phase instead of other phases, such as anatase and brookite, could be attributed to the small lattice mismatch between FTO and rutile. Both rutile and SnO_2 have near identical lattice parameters with a =4.594, c = 2.958 and a = 4.737, c = 3.185 for TiO_2 and SnO_2, respectively, making the epitaxial growth of rutile TiO_2 on FTO film possible. On the other hand, anatase and brookite have lattice parameters of a = 3.784, c = 9.514 and a =5.455, c = 5.142, respectively. The production of these phases is unfavorable due to a very high activation energy barrier which cannot be overcomed at the low temperatures used in this hydrothermal reaction.

Exp. Theo. NANOTECHNOLOGY 4 (2020) 47-58

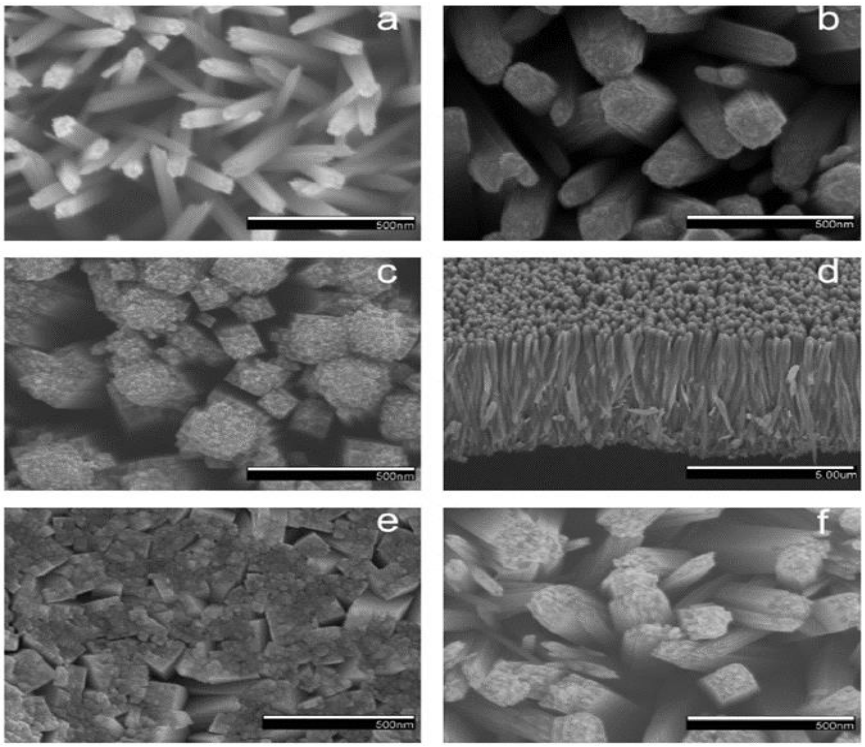

Figure 1 FESEM images of TiO_2 nanorods grown at 180 1C for 2 h with different amounts of titanium tetrachloride in static solutions of 40 mL hydrochloric acid and 50 mL deionized water: (a) 0.3 mL, (b) 0.4 mL, (c) 0.5 mL top view, (d) 0.5 mL cross-sectional view, (e) 1.0 mL of titanium tetrachloride, (f) 0.3 mL of titanium tetrachloride in a solution of 35 mL hydrochloric acid and 55 mL deionized water.

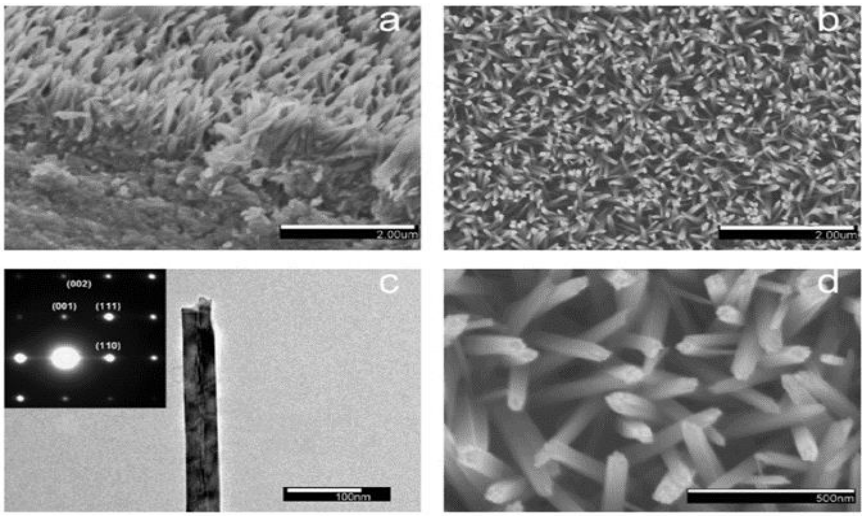

Figure 2 FESEM images of TiO_2 nanorods; (a) cross-sectional view, (b) top view, (d) high magnification view. (c) TEM image of a single- crystalline TiO_2 nanorod and corresponding SAED pattern.

Exp. Theo. NANOTECHNOLOGY 4 (2020) 47-58

3.2 Deposition of CdS quantum dots

Compared to conventional bulk semiconductors, the relaxa- tion rate of photo-generated excitonic states in quantum dots is much slower due to a 'phonon bottleneck' effect, which has been observed in quantum dots by a research group at NREL [31], allowing MEG to become dominant in QDs. Also, to increase utilization of photon energy in the visible light region, the band gap of the semiconducting material used for QD sensitization must fall within the range of 0.5 eV–3.5 eV. CdS was chosen as an ideal system for sensitization because the MEG phenomenon in CdS QDs has been well-studied [32–34]. CdS quantum dots were deposited onto the surface of TiO_2 nanorods by chemical bath deposition (CBD) under ultrasonic environment in alcohol solvents. It is noteworthy that the deposition rate of the CdS assembled in the alcohol system is much higher than in aqueous solutions [35]. Figs. 3a–b and c–d show typical FESEM and TEM images of the CdS QDs deposited onto TiO_2 nanorods. The CdS QDs are typically 5–10 nm in diameter with uniform coverage of the TiO_2 nanorod surface. Selected area electron diffraction (SAED) of the CdS coated TiO_2 nanorod (Fig. 3c) shows clear spot diffraction patterns due to the high crystallinity of the tetragonal rutile TiO_2 nanorod, as well as rings characteristic of the greenockite CdS QDs. To obtain a thick layer of CdS QDs for better XRD characterization, CdS QDs were deposited onto bare glass substrates for more than 10 CBD cycles. XRD patterns of an as-deposited CdS QD layer also indicate a crystalline hexagonal greenockite structure [SI 2].

The advantage of our synthetic method is that the CdS quantum dots make direct contact with the TiO_2 nanorod surface. The CdS QDs form a firm connection on the TiO_2 nanorods with a type-II heterojunction that greatly enhances charge transport, charge separation, and overall photocurrent efficiency of our solar device. Also, CBD under ultrasonic agitation greatly enhanced the speed of CdS quantum dot deposition. SEM images are presented for CdS deposition with and without ultrasonic assistance after 5 CBD cycles [SI 3]. The improved performance of CdS QDSSC Enhanced absorption of visible light by the CdS@TiO_2 struc- ture was confirmed by UV–visible spectroscopy (Fig. 4a). The CdS@TiO_2 structure showed a higher absorption coeffi- cient compared to bare TiO_2 nanorods over the entire visible light spectrum. The evident increase in light absorption after CBD of CdS QDs is evident around 400 nm and 540 nm. The CdS@TiO_2 showed an apparent increase in absorption of the visible light ranging from 400 to 550 nm. This increase in absorption is mainly due to the layer of CdS QDs deposited onto the TiO_2 nanorod, as this absorption edge is close to the band gap of CdS (E =2.45 eV).

Fig. 4b shows UV–visible transmission spectroscopy obtained from the CdS@TiO_2 samples prepared through various CBD cycles. Increased visible light absorption was observed with increase in CBD cycle, indicating an increased amount of CdS deposition. Compared to other works, the redshift of the absorption edge and onset position with increased CBD cycle is negligible with increased CBD cycle implying the size growth of CdS QDs is impeded with ultrasound agitation. In the first few CBD process, TiO_2 nanorod surface is not completely covered by CdS QDs; after 5 CBD cycles CdS QD layer thickness growth become dominant and surface is fully covered with a layer of CdS. Low coverage of the TiO_2 surface give rise to a low light absorption resulting in low

Exp. Theo. NANOTECHNOLOGY 4 (2020) 47-58

efficiency; on the other hand, excess of CdS QDs hinders both charge transport and diffusion of the electrolyte also increases the recombination of photoexcited carriers in the interfacial area between the QD consequently resulting in low overall efficiency [36].

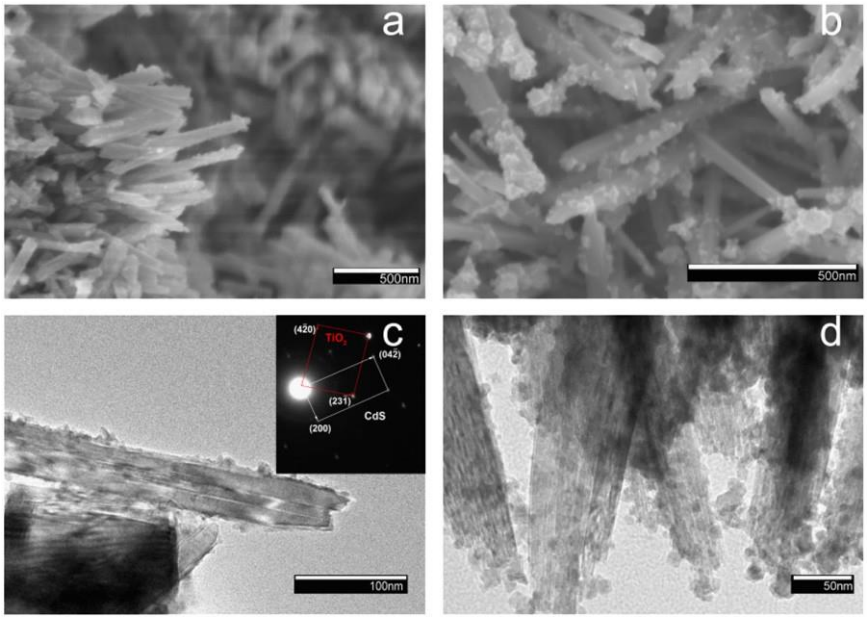

Figure 3 FESEM images of (a) cross-sectional and (b) top view of CdS QD coated TiO_2 nanorods. (c) TEM image of a CdS QD coated TiO_2 nanorod and corresponding SAED pattern. (d) TEM image of CdS QDs deposited onto TiO_2 nanorods.

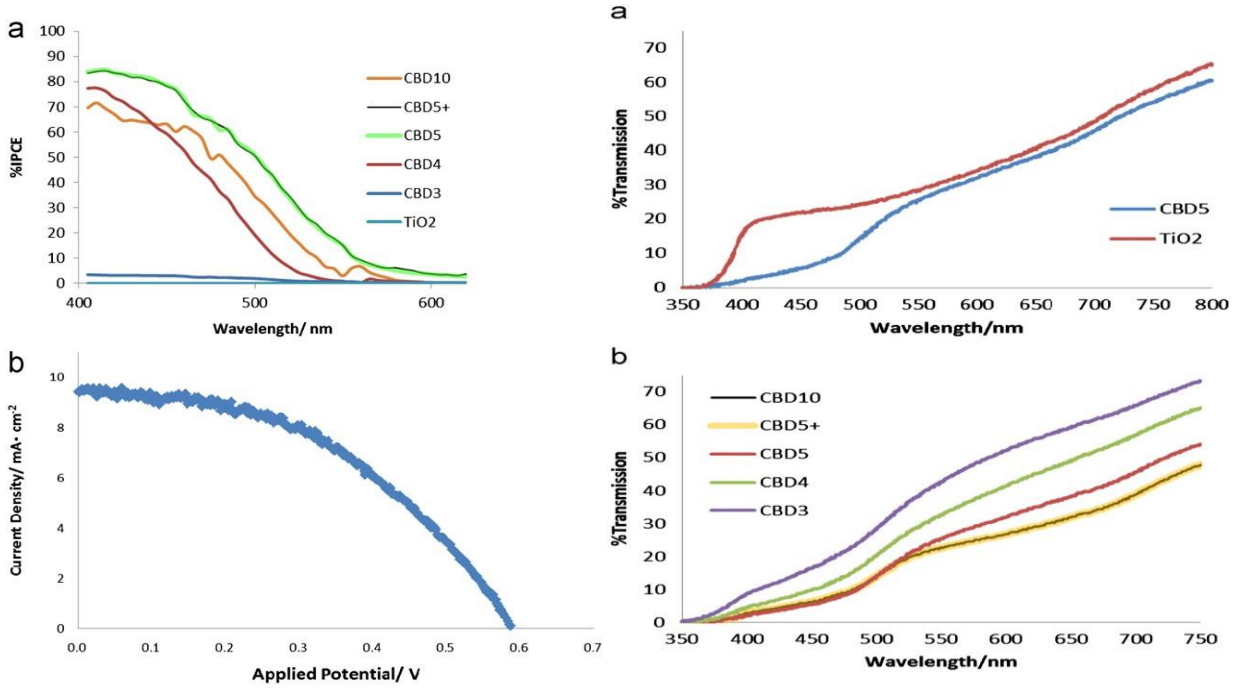

Figure 4 (a) UV–visible transmission spectra of bare TiO_2 nanorod arrays (red) and CdS QD coated TiO_2 nanorod arrays (blue). (b) UV–visible transmission spectra of CdS QD coated TiO_2 nanorod arrays obtained after various CBD cycles.

The incident photon to current conversion efficiencies (IPCE) obtained from QDSSCs assembled using various electrodes prepared through different CBD cycles are shown in Fig. 5a. By using the S/S^{2-} redox couple electrolyte, IPCE values as high as 85% can be obtained for wavelength in the visible light region with 5 CBD cycles. An increase in CBD cycles is followed by an increase in IPCE over the entire visible light region, implying that the CdS QDs play a major role in photon- to-electron conversion. After 5 CBD cycles, the IPCE drops slightly and when reaching 10 CBD cycle, IPCE drops even lower especially in the 400–500 nm visible light region where CdS QDs play a major role in modifying absorption spectra. The photocurrent–voltage (*I–V*) curves of the QDSSC were measured under one sun illumination (AM1.5, 100 mW/cm^2). An max- imum efficiency of 2.54% was obtained with a CdS@TiO_2 sample prepared with 5 CBD cycles (Fig. 5b).Compared with the reported results, the efficiency of CdS QDSSCs obtained using single crystalline TiO_2 nanorods is higher than using conventional mesoporous TiO_2 films (1.84%) [37]; the efficiency of CdS QDSSC acquired through wet-chemical approaches showed higher performance than CVD equivalents (1.51%) [38]. This may be attributed to better size control of CdS QDs and optimized adhesion between the CdS QDs and TiO_2 nanorods. CdS QDSSCs constructed through this wet-chemical approach showed superior performance compared to recent reports [36–38].

Although the efficiency obtained with this CdS QDSSC is still low compared with Graetzel Cells using dye sensitizers, Fig. 5 (a) IPCE spectra of CdS QD coated TiO_2 nanorod arrays obtained after various CBD cycles. (b) Current–voltage (*I–V*) characteristics of CdS QD coated TiO_2 nanorod arrays obtained after 5 CBD cycles. the CdS QDSSCs presented in our work provide advantages that are not available in DSSCs. First, the use of quantum dots offers the ability to adjust absorption spectra by tuning CdS QD sizes. Second, the photochemical stability of CdS quantum dots is more desirable compared to organic dyes. Third, exploiting the multiple exciton generation (MEG) effect with CdS QDs offers the opportunity to surpass the Shockley– Queisser limit [39]. This study opens a possibility to use a 3D nanostructured material with a facile wet-chemical approach for QDSSC studies. In the present study, the low efficiency of the CdS QDSSC is limited by narrow-range absorption of CdS QDs in the visible light region and the low transport efficiency of the S/S^{2-} redox couple. By applying sensitizing materials with narrower band gaps and a more efficient redox couple electrolyte, higher cell efficiency could be achieved.

4. CONCLUSIONS

Single-crystalline TiO_2 nanorod arrays with practical length (1–2 mm) and density (20 nanorods/mm^2) were successfully grown on fluorine-doped tin oxide (FTO) glass substrates by a facile hydrothermal approach. CdS quantum dots with a size of 5–10 nm was deposited onto a TiO_2 nanorod surface using ultrasound assisted chemical bath deposition (CBD). The CdS@TiO_2 heterojunction showed a notable increase in visible light absorption, enhanced incident photon-to-current conversion efficiency (IPCE) as high as 85% can be obtained for wavelength in the visible light region. Quantum-dot sensitized solar cells (QDSSC) constructed with CdS@TiO_2 structures operated at 2.54% power conversion efficiency. The performance

of CdS QDSSCs is approaching the efficiencies of dye-sensitized solar cells (DSSC), providing an alternative solution in solar cell design and fabrication.

References

[1] Ali H. AL-Hamdani, Mohammed A.R. Hussein, Aya H. Makki, Exp. Theo. NANOTECHNOLOGY 3 (2019) 1
[2] M. Gratzel, Nature 414 (2001) 338
[3] M.J. Currrie, J.K. Mapel, T.D. Heidel, S. Goffri, M.A. Baldo, Science 321 (2008) 226
[4] B. Eva, C.K. Frederik, Solar Energy Materials and Solar Cells 91 (2007) 954
[5] G. Serap, N. Helmut, S.S. Niyazi, Chemical Reviews 107 (2007) 1324
[6] Y.J. Cheng, S.H. Yang, C.S. Hsu, Chemical Reviews 109 (2009) 5868
[7] R.R. King, Nature Photonics 2 (2008) 284
[8] W. Guter, J. Schone, S.P. Philipps, M. Steiner, G. Siefer, A. Wekkeli, E. Welser, E. Oliva, A.W. Bett, F. Dimroth, Applied Physics Letters 94 (2009) 223504
[9] J. Geisz, S. Kurtz, M.W. Wanlass, J.S. Ward, A. Duda, D.J. Friedman, J.M. Olson, W.E. McMahon, T.E. Moriarty,J.T. Kiehl, Applied Physics Letters 91 (2007) 023502
[10] B. Liu, E.S. Aydil, Journal of the American Chemical Society 131 (2009) 3985
[11] K.S. Leschkies, R. Divakar, J. Basu, E. Enache-Pommer, J.E. Boercker, C.B. Carter, U.R. Kortshagen, D.J. Norris, E.S. Aydil, Nano Letters 7 (2007) 1793
[12] L.M. Peter, D.J. Riley, E.J. Tull, K.G.U. Wijayantha, Chemical Communications 10 (2002) 1030
[13] A.J. Nozik, Chemical Physics Letters 457 (2008) 3
[14] A. Luque, A. Marti, A.J. Nozik, MRS Bulletin 32 (2007) 236
[15] P.V. Kamat, Journal of Physical Chemistry C 112 (2008) 18737
[16] D.R. Baker, P.V. Kamat, Advanced Functional Materials 19 (2009) 805
[17] S.K. Haram, B.M. Quinn, A.J. Bard, Journal of the American Chemical Society 123 (2001) 8860
[18] G.K. Mor, K. Shankar, M. Paulose, O.K. Varghese, C.A. Grimes, Nano Letters 6 (2006) 21
[19] K. Zhu, N.R. Neale, A. Miedaner, A.J. Frank, Nano Letters 7 (2007) 69
[20] H. Wang, Y.S. Bai, H.Z.H. Zhang, Zhang, J.H. Li, L. Guo, Journal of Physical Chemistry C 114 (2010) 16451
[21] J.J. Wu, C.C. Yu, Journal of Physical Chemistry B 108 (2004) 3377
[22] C. Weng, K.F. Hsu, K.H. Wei, Chemistry of Materials 16 (2004) 4080
[23] A. Kongkanand, K. Tvrdy, K. Takechi, M. Kuno, P.V. Kamat, Journal of the American Chemical Society 130 (2008) 4007
[24] I. Robel, V. Subramanian, M. Kuno, P.V. Kamat, Journal of the American Chemical Society 128 (2006) 2385
[25] V. Gonza'lez-Pedro, X. Xu, I. Mora-Sero´, J. Bisquert, ACS Nano 4 (2010) 5783
[26] T. Toyoda, K. Oshikane, D. Li, Y. Luo, Q. Meng, Q. Shen, Journal of Applied Physics 108 (2010) 114340
[27] T. Sugimoto, X. Zhou, A. Muramatsu, Journal of Colloid and Interface Science 259 (2003) 43
[28] C. Lee, Y.M. Sung, T.G. Kim, H. Choi, Applied Physics Letters 91 (2007) 113104
[29] J.L. Blackburn, D.C. Selmarten, A.J. Nozik, Journal of Physical Chemistry B 107 (2003) 14154
[30] Y. Wada, H. Kuramoto, J. Anand, T. Kitamura, T. Sakata, H. Mori, S. Yanagida, Journal of Materials Chemistry 11 (2001) 1936

[31] P.H. Mugdur, Y.J. Chang, S.Y. Han, Y.W. Su, A.A. Morrone, S.O. Ryu, T.J. Lee, C.H. Chang, Journal of the Electrochemical Society 154 (2007) 482
[32] Y.J. Shen, Y.L. Lee, Nanotechnology 19 (2008) 045602
[33] H. Chang, Y.L. Lee, Applied Physics Letters 91 (2007) 053503
[34] S. Hachiya, Y. Onishi, Q. Shen, T. Toyoda, Journal of Applied Physics 110 (2011) 054319
[35] Y.L. Lee, C.H. Chang, Journal of Power Sources 185 (2008) 584
[36] C. Lee, T.G. Kim, W. Lee, S.H. Han, Y.M. Sung, Crystal Growth and Design 9 (2009) 4519
[37] W. Shockley, H.J. Queisser, Journal of Applied Physics 32 (1961) 510

Exp. Theo. NANOTECHNOLOGY 4 (2020) 47-58